Materials Chemistry

Cite this: *J. Mater. Chem.*, 2012, **22**, 8896

www.rsc.org/materials

PAPER

Designing materials by means of the cavity-microelectrode: the introduction of the quantitative rapid screening toward a highly efficient catalyst for water oxidation†

Alessandro Minguzzi,* Cristina Locatelli, Giuseppe Cappelletti, Claudia L. Bianchi, Alberto Vertova, Silvia Ardizzone and Sandra Rondinini*

Received 9th November 2011, Accepted 2nd March 2012
DOI: 10.1039/c2jm15750k

In this paper, we introduce the concept and the methodology of quantitative rapid screening (QRS) of catalysts. It is based on the use of the cavity-microelectrode (C-ME), a tool that hosts a known amount of powder and can be filled and emptied quickly, thus allowing the quantitative, rapid, fine characterization of different materials. Here, C-MEs are used for selecting a suitable material to be used as electrocatalyst for the oxygen evolution reaction (water oxidation) in acidic environment, a key process for the majority of the industrial electrolytic applications including the production of high purity hydrogen. A matrix of materials, each having the same low iridium oxide content, is quantitatively screened for finding the most promising one. C-MEs allowed us to measure the effective number of active Ir sites and their surface concentration. The success of this strategy is proven by the good performance of the "best" material when tested in a proton exchange membrane water electrolyzer, that allowed high hydrogen fluxes at a low cell potential (~4000 $dm^3\ h^{-1}\ m^{-2}$ at less than 1.9 V).

Introduction

Research in catalysis always faces the need of testing several materials, each having unique chemical or morphological properties (chemical and phase composition, morphology, specific surface area). Besides, catalysis often requires the design of composite materials.

The increasing importance that electrocatalysis[1] has assumed during the last decades is mainly due to its role in environmental protection[2,3] and energy conversion processes/devices like fuel cells, water electrolysis (either driven by sunlight or by electric energy) and CO_2 reduction.

For each of these reactions, the scientific literature is quite wide: for example, the oxygen reduction reaction (ORR, at the bases of most of the fuel cell systems) is the key subject of dozens of thousands of papers, most of them related to the study of a single material or of a small group of them. Consequently, the research of suitable electrochemical rapid screening methods for the rapid evaluation of material libraries have been so popular in the last decade.[4–10] Among them, scanning electrochemical microscopy (SECM) has allowed the design of innovative electrocatalysts for both the oxygen evolution and reduction reactions, as well as of materials for photoelectrochemical devices. Other methods for rapid screening were designed to enable spectroelectrochemical analysis together with the electrochemical one.[11] Despite their excellent sensitivity, the electrochemical rapid screening methods described so far usually provide as output quantity a reaction rate, which includes implicitly the chemical and morphological properties of the studied materials. However, the rapid screening methods would be much more powerful if the relevant properties of each material could be either known or – even better – determined during the rapid screening itself. For this task, the unique properties of microelectrodes, which have proven to be key tools for designing innovative techniques, can be successfully exploited to acquire otherwise inaccessible specific information. An example is provided by the recently developed surface interrogation mode of SECM.[12–15]

In the present contribution, we propose a new strategy for finding new and effective electrocatalysts, based on the novel general concept of quantitative rapid screening. This strategy is developed by using the cavity-microelectrode (C-ME),[16–18] *i.e.* a recessed microdisk that can host a known amount of material. Notwithstanding C-MEs were introduced 18 years ago, we demonstrated in a recent publication[19] that the operational volume of a C-ME can be accurately determined, thus allowing the normalization of any extensive property for the amount of the sample under investigation. Here we will demonstrate that this feature can be exploited for the rapid screening of material libraries by following an innovative approach, according to which

Dipartimento di Chimica Fisica ed Elettrochimica, Università degli Studi di Milano, via Golgi 19, 20133 Milan, Italy. E-mail: alessandro.minguzzi@unimi.it; sandra.rondinini@unimi.it

† Electronic supplementary information (ESI) available: Additional experimental details. See DOI: 10.1039/c2jm15750k

the use of C-MEs leads to the determination of the specific number of active sites and, if needed, to a good estimation of turnover frequencies. It is worth noting that the final results of the screening are in terms of intensive quantities, not influenced by geometrical factors (*e.g.* specific surface area, number of active sites) but only by the intrinsic activity of every single material (chemical composition, nature of the active sites, synergistic effects).

This method is applied here to the case of iridium oxide-based materials as effective electrocatalysts for water oxidation (the oxygen evolution reaction, OER) in acidic media.[20,21]

We selected the proton-coupled-electron-transfer (PCET)[22] reaction because its importance spans from industrial applications (*e.g.*, photo- or electro-driven production of high purity hydrogen) to life-science aspects (*e.g.* photosynthesis). In addition, OER kinetics always represent the limiting factor in any system in which it is involved. This situation is complicated by the harsh conditions at which the catalysts operate, especially when conducted under acidic conditions. For all these reasons, publications on catalysts for water oxidation recently gained a lot of attention.[4,23–27]

In this work, we compare different IrO_2–SnO_2 mixed oxides (at constant Ir molar fraction) prepared by the sol–gel technique and following different synthetic routes to purportedly obtain final materials having markedly different properties. The use of C-MEs allows us to finely distinguish the properties of these materials, notwithstanding their (apparently) most influential property, *i.e.* their chemical composition, is kept constant and low (15 mol% of IrO_2). All materials have been screened in a potential window in which iridium oxide shows pseudocapacitive–solid state redox transitions of the type:

$$MO_x(OH)_y + \delta H^+_{(solution)} + \delta e^-_{(oxide)} \rightarrow MO_{x-\delta}(OH)_{y+\delta} \quad (1)$$

which is at the basis of the electrochemical properties of many conductive oxide materials.[28]

Moreover, in a recent paper[19] we quantitatively demonstrated that the number of sites that participate in reaction (1) is proportional to the number of sites on which OER occurs:

$$2H_2O \rightarrow O_2 + 4H^+ + 4e^- \quad (2)$$

The central point of this paper is the quantitative rapid screening (QRS) implemented for the comparison of different materials with the final goal of selecting a high activity–low cost IrO_2–SnO_2 mixed oxide, at low iridium content (15 mol%), in terms of the number of sites that participate in reaction (1).

To further prove this, the selected powder has been used for preparing an operative electrode to be used in a proton exchange membrane water electrolyzer (PEM-WE), that represents the most promising system for producing high purity hydrogen from renewable sources.

This material allowed the water electrolysis at 10 kA m^{-2} at less than 1.9 V, in line with the most recent advanced studies.[29]

Experimental

Synthesis of IrO_2–SnO_2 powder

The SnO_2 particles were obtained by a room-temperature sol–gel reaction, as previously reported,[30] adopting tin *tert*-butoxide ($Sn(OC(CH_3)_3)_4$, purchased from Aldrich, 99.99% purity) as the tin source. Alternatively, we adopted a precipitation method starting from $SnCl_4$ (Aldrich, 99.995%) by addition of NH_3 up to pH 6, followed by centrifugation and drying (80 °C) steps. The Ir dopant (from $IrCl_3$ hydrate, purchased from Alfa Aesar 99.9%) was added to the SnO_2 xerogel matrix in order to reach a final composition of $x_{IrO_2} = 0.144$ (nominal Ir/Sn molar ratio = 0.18). The addition was performed in three different ways, as follows:

(a) directly in the sol–gel/precipitation syntheses (co-synthesis, CS);

(b) by the impregnation (IMP) method by using $IrCl_3$ dissolved in a few ml of diluted aqueous HCl, mixed with 2-propanol. Finally the solvent was removed by using a Rotavapor® set at 40 °C;

(c) by mechanical mixing (MM) of $IrCl_3$ with the tin oxide xerogel in an agate mortar for 10 min.

After the Ir addition, all materials were calcined under oxygen flux (50 NL h^{-1}) for 2 hours at the selected temperature (450 or 500 °C), reached with a 3 hour ramp. Only in the case of powders obtained by chloride precursor a dialysis procedure in water was performed after the calcination step to remove the NH_4Cl salt. The pure IrO_2 sample was prepared by calcination at 500 °C under oxygen flux (50 NL h^{-1}) for 2 hours of $IrCl_3$, that was previously finely ground for 10 minutes. The synthetic procedure is summarized in each powder name as follows:

tin precursor (Alk = alkoxide, Cl = chloride)-
$Ir_{(method\ of\ Ir\ addition)}$_calcination temperature.

The synthesis of the best performing material, Alk-Ir_{IMP}_450, was repeated twice (samples (1) and (2)) for reproducibility. The electrochemical characterization was performed on both samples ((1) and (2)). In particular, sample (2) was also used to set up the C-ME preparation and characterization as described by Locatelli *et al.*[19]

Samples characterization

Room temperature X-ray powder diffraction (XRPD) patterns were collected between 20 and 80° (2θ range; $\Delta 2\theta = 0.02°$, time per step = 10 s, scan speed = 0.002° s^{-1}) with a Siemens D500 Diffractometer, using Cu Kα radiation. The Rietveld refinement has been performed using the GSAS software suite[31] and its graphical interface EXPGUI.[32] The backgrounds have been subtracted using a shifted Chebyshev polynomial. The profile of the diffraction peak has been fitted with a pseudo-Voigt profile function. Site occupancies and the overall isotropic thermal factors have been varied. The average diameter of the crystallites, *d*, was estimated from the most intense reflection of the SnO_2 cassiterite phase using the Scherrer equation.

Specific surface areas were determined by the classical BET procedure using a Coulter SA 3100 apparatus. Desorption isotherms were used to determine the pore size distribution using the Barret–Joyner–Halander (BJH) method.

X-ray photoelectron spectroscopy spectra were obtained using an M-probe apparatus (Surface Science Instruments). The source was monochromatic Al Kα radiation (1486.6 eV). A spot size of 200 μm × 750 μm and pass energy of 25 eV were used. 1s level hydrocarbon-contaminant carbon was taken as the internal reference at 284.6 eV. For each sample, survey analyses in the whole range of the X-ray spectrum have been performed.

Cavity-microelectrode preparation and characterization

The preparation of C-MEs and the determination of their operative geometry is exhaustively described in ref. 19.

Cyclic voltammetry

All powders are tested by cyclic voltammetry after being inserted into a cavity-microelectrode as described in more detail in ref. 19.

All measurements are performed in 0.5 M H_2SO_4 or in 1 M $HClO_4$. All solutions are prepared with Milli-Q grade water.

For all samples, a common procedure is followed:

(1) Fill the C-ME with the powder and record of a CV at 20 mV s^{-1}.

(2) Repeat (1) for at least three times, to assess the reproducibility of the different fillings.

(3) Record CVs at 20, 10, 5 and 2 mV s^{-1}.

Preparation and test of membrane electrode assemblies (MEAs)

A 5 × 5 cm^2 piece of cationic membrane (Nafion® 115) was first boiled in pure water (2 h), then in aqueous 0.5 M H_2SO_4 (1 h) and again in water (3 h) before being immersed in a 20 wt% aqueous solution of triethanolamine (purchased from VWR Int., 97% purity) for 24 hours.[33]

A MEA is then prepared by spraying the desired amount of powder (previously dispersed into 2-propanol, adopting a fixed amount (mg) of powders/volume (ml) of solvent equal to 10) onto the dried membrane. During the spraying the membrane is kept warm (at about 70 °C) for the rapid solvent evaporation. The role of the triethanolamine is to reduce the membrane volume variation that follows its drying/hydration.

The final powder loading onto the membrane was set to 1 mg cm^{-2} for the cathodic (platinum E-TEK 28.6 wt%) layer 1.2 mg cm^{-2} of IrO_2 on the anodic layer. The geometric active area is 7.1 cm^2.

After the electrocatalysts deposition, the MEA was hot-pressed at 100 °C, 176 kg cm^{-2} for 5 minutes. The MEA was then rinsed and immersed in water (24 hours), then in $HClO_4$ 0.1 M (48 h) and again in water (24 h). The MEA was then mounted into the electrolyzer cell and tested by application of constant current densities (considering the geometrical area of the exposed portion of the deposit) by using an ELIND DC regulated power supply (0–60 V). The potential was read by using an AMEL Instrument model 1426 four channel electrometer, whose output signal was recorded by a PC.

The electrochemical cell consists of two graphite blocks designed for being used as current collectors and water flow plates. Water is heated in a separate reservoir at the desired temperature before each experiment and is fluxed through the cell, thanks to two peristaltic pumps.

Results and discussion

Physicochemical characterization

Fig. 1 reports the X-ray diffraction lines of three samples calcined at 450 °C, obtained from the alkoxide precursor by different Ir addition procedures. For powders obtained by co-synthesis (CS) (Fig. 1a) the XRD pattern shows only the peaks of the SnO_2 cassiterite structure, indicating the formation of a SnO_2–IrO_2 solid solution.[30] In the case of the two samples obtained by impregnation (IMP) (Fig. 1b) and mechanical mixing (MM) (Fig. 1c), the presence of an appreciable amount of separate IrO_2 phase (around 5–8 wt%) leads to a modification of the relative intensity ratio of the two most intense peaks (centered at 26.7° and 34.1°, respectively). Fig. 1d reports the fitting of the lower angle portion of Alk-Ir_{IMP}_450 sample, in which the 2θ positions of the most intense reflections of the two phases are indicated (SnO_2 [1 1 0] 100% at 26.7° and [1 0 1] 80.2% at 33.9°; IrO_2 [1 1 0] 100% at 27.9° and [1 0 1] 96.8% at 34.6°). This effect becomes more appreciable for powders obtained by MM addition of the Ir precursor to the tin xerogel (from tin chloride), calcined at 500 °C (Fig. S1d, ESI†), in which the two phases give rise to separate peaks (1 1 0 plane for both oxides) respectively at 26.7° and 27.7°. The crystallite sizes, obtained by elaboration of the fitted X-ray peaks by the Scherrer's equation, are in all cases quite small (around 4–5 nm) and close to the determination threshold. The only exception is represented by sample Cl-Ir_{IMP}_500, which shows the largest crystallite size (around 20 nm).

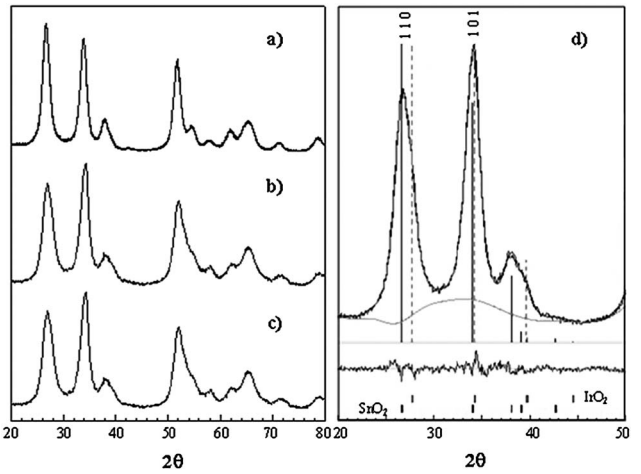

Fig. 1 Powder X-ray diffraction lines of samples obtained by alkoxide precursor, Ir-doped by (a) co-synthesis (Alk-Ir_{CS}_450), (b) impregnation (Alk-Ir_{IMP}_450) and (c) mechanical mixing (Alk-Ir_{MM}_450) procedures, calcined at 450 °C; (d) fitting curve of the lower angle portion of Alk-Ir_{IMP}_450 sample together with the 2θ position of most intense *h k l* planes of the SnO_2/IrO_2 phases.

Table 1 reports the experimental surface area, the total pore volume and the relative pore size distribution of all synthesized samples. As a general trend the specific surface area and the relative total pore volume are larger for calcinations at 450 °C than 500 °C, as expected. Only in the case of samples obtained by MM (at both temperatures) the specific surface areas are lower than in the case of the other synthetic procedures. Fig. S2, ESI† shows representative nitrogen adsorption isotherms with the relative hysteresis loop for three samples obtained from the alkoxide precursor and calcined at 450 °C. The observed hysteresis is characteristic of mesoporosity.[34] By applying the BJH (Barrett, Joyner, Halenda) model[35] based on capillary condensation in mesopores, the mesopore size distribution is obtained (Table 2). The present shape of the hysteresis loops can be classified as type E, which is associated with capillary condensation in "ink bottle" pores, *i.e.* pores having narrow

Table 1 BET surface area, total pore volume with the relative pore size distribution and Ir/Sn atomic ratio by XPS determination for all the synthesized samples

			% V_{pore}					
Sample	S_{BET} ($m^2\ g^{-1}$)	V_{pore} ($ml\ g^{-1}$)	<6 nm	6 < d < 10 nm	10 < d < 20 nm	20 < d < 80 nm	>80 nm	Ir/Sn
Alk_450	64 ± 2	0.097	89.0	2.8	3.1	3.6	1.5	—
Alk_500	52 ± 1	0.092	90.0	2.2	2.1	3.2	2.5	—
Alk-Ir_{CS}_450	80 ± 2	0.054	85.0	5.0	2.8	3.7	3.5	0.13
Alk-Ir_{CS}_500	58 ± 1	0.079	76.3	14.8	4.1	3.4	1.4	0.14
Alk-Ir_{IMP}_450 (1)	79 ± 2	0.080	65.3	5.3	7.1	14.7	7.6	1.45
Alk-Ir_{IMP}_500	57 ± 1	0.081	50.4	28.6	5.5	8.4	7.1	1.39
Alk-Ir_{MM}_450	66 ± 1	0.077	69.5	3.9	6.7	12.9	7.0	n.d.
Alk-Ir_{MM}_500	47 ± 1	0.085	37.6	36.6	6.8	10.5	8.5	n.d.
Cl-Ir_{IMP}_450	82 ± 2	0.080	78.5	5.4	4.0	7.7	4.4	0.32
Cl-Ir_{IMP}_500	59 ± 1	0.095	61.4	25.2	3.8	6.3	3.3	0.31
Cl-Ir_{MM}_500	42 ± 1	0.047	33.4	41.2	4.1	11.6	9.7	n.d.
IrO_2_500	67 ± 1	0.114	44.5	9.8	10.9	22.2	12.6	—

Table 2 Molar fraction, "total" (Q_{tot}) and "outer" (Q_{out}) quantities of charge relevant to the densities of sites, further elaboration of Q_{tot} and Q_{out} data for all the materials screened by C-ME. Standard deviations are obtained adopting the error propagation theory

Sample	x_{IrO_2}	Q_{tot}/nC μm^{-3}	Q_{out}/nC μm^{-3}	Q_{out}/Q_{tot}	$Q_{tot}/Q_{tot\ IrO_2\text{-}500}$	$n_{s,tot}$/mol g^{-1}	$n_{s,out}$/mol g^{-1}
Alk-Ir_{IMP}_450 (1)	0.144	0.107 ± 0.011	0.095 ± 0.010	88.8	0.58	9.45×10^{-5}	8.41×10^{-5}
Alk-Ir_{IMP}_450 (2)	0.144	0.097 ± 0.004	0.087 ± 0.003	90.1	0.52	8.56×10^{-5}	7.72×10^{-5}
Alk-Ir_{IMP}_500	0.144	0.088 ± 0.013	0.075 ± 0.008	85.3	0.48	7.79×10^{-5}	6.65×10^{-5}
Alk-Ir_{MM}_450	0.144	0.093 ± 0.019	0.070 ± 0.018	76.1	0.50	8.07×10^{-5}	5.99×10^{-5}
Alk-Ir_{MM}_500	0.144	0.060 ± 0.008	0.036 ± 0.005	59.3	0.33	5.34×10^{-5}	3.17×10^{-5}
Alk-Ir_{CS}_450	0.144	0.034 ± 0.002	0.016 ± 0.002	46.0	0.19	3.03×10^{-5}	1.40×10^{-5}
Alk-Ir_{CS}_500	0.144	0.024 ± 0.002	0.013 ± 0.002	53.5	0.13	2.09×10^{-5}	1.12×10^{-5}
Cl-Ir_{IMP}_450	0.144	0.044 ± 0.008	0.025 ± 0.004	56.9	0.24	3.91×10^{-5}	2.23×10^{-5}
Cl-Ir_{IMP}_500	0.144	0.033 ± 0.005	0.017 ± 0.006	51.4	0.18	2.92×10^{-5}	1.50×10^{-5}
Cl-Ir_{MM}_500	0.144	0.048 ± 0.003	0.048 ± 0.002	99.4	0.26	4.25×10^{-5}	4.22×10^{-5}
IrO_2_500	1	0.184 ± 0.019	0.169 ± 0.007	91.6	1.00	1.11×10^{-4}	1.01×10^{-4}

necks and wide bodies. The three samples give rise to a common loop shape and to a comparable size distribution of the pores.

Cyclic voltammetry of powders hosted in cavity-microelectrodes

In a recent paper,[19] we demonstrated that, thanks to the use of C-MEs for the quantitative evaluation of the properties of electrodic powder materials, the number of sites involved in the solid-state, pseudocapacitive phenomenon (eqn (1)) are proportional to those involved in the OER, possibly because both processes involve the proton exchange with the solution. This is the reason why all CVs were conducted in the 0.4–1.4 V *vs.* RHE potential window, where capacitive and pseudocapacitive processes are predominant.

Fig. 2 shows a sequence of CVs recorded in a C-ME having an operative volume equal to 103.6 ± 4.4 μm^3 (ref. 19) containing samples of the powder marked as Alk-Ir_{IMP}_450 (2). The figure proves the rather good reproducibility of the filling/emptying of the cavity and in turn, of the relevant voltammetric signals. In all CVs, the "bumps" observed in the scanned potential window account for the processes described by eqn (1).

Note that any CV obtained using C-ME as powder support does not suffer from typical experimental drawbacks like the contributions of ohmic drop and of the current collector material, which often influence the results.[36] In turn, this allows a fine analysis of the electrochemical features of each tested material, in relationship with the other physico-chemical properties, a discussion which, however, is beyond the goal of this work.

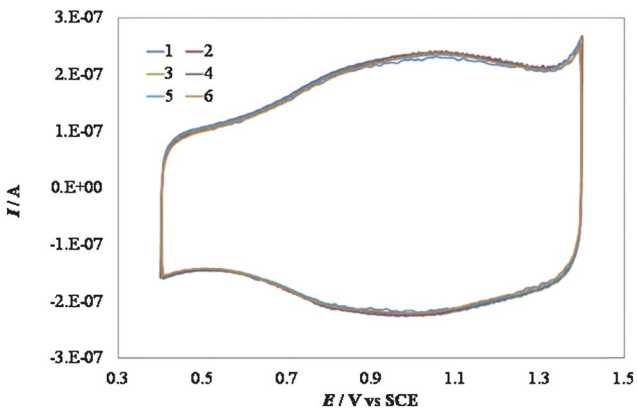

Fig. 2 Cyclic voltammograms of Alk-Ir_{IMP}_450 (2) inserted into a C-ME. Each CV refers to a different filling of the same C-ME. All CVs are recorded in 0.5 M H_2SO_4. Scan rate: 20 mV s^{-1}.

As already reported by different authors, the analysis of the voltammetric charge in dependence on the potential scan rate leads to the evaluation of the availability of active sites. This is considered as the best *in situ* method for the determination of the number of available active sites of metallic oxides.

In particular, the sites involved at high scan rates, v, accounts for the Q_{out} value, that represents the number of sites that react more quickly, while the limit at $v \rightarrow 0$ gives the total number of sites, Q_{tot}.[37–39] For a more detailed explanation of the determination of Q, the reader is invited to read the supporting information of a recently published work by some of us.[40]

Thanks to the exact knowledge of the volume of the powder under investigation, it is possible to calculate the specific moles of Ir sites that participate in eqn (1). The comparison of this parameter with the specific nominal iridium oxide content gives the percentage of iridium sites that actually are able to exchange protons with the solution.[41]

Table 2 collects the relevant results and reports: the nominal iridium oxide content (molar fraction), x_{IrO_2}; Q_{tot} and Q_{out}, with their standard errors, and already normalized by each powder volume; the Q_{out}/Q_{tot} ratio; the $Q_{tot}/Q_{tot,IrO_2\text{-}500}$ ratio and the specific number of sites, n_s (mol g^{-1}). All Qs are normalized to the operational volume of the CME used as powder holder, therefore the units are expressed in nC μm^{-3}. The results clearly reflect the striking differences between the various materials together with some common features. The role of the calcination temperature is easily discussed: for each combination of preparation method/tin precursor, increasing the calcination temperature leads to a parallel decrease of the specific surface area (determined by N_2 adsorption/desorption) and of Q_{tot} that represents the "electrochemical" surface area. The effect of the nature of the precursor salts is less straightforward; materials obtained from $SnCl_4$ show values of the density of total available sites usually lower than from Sn(t-BuO)$_4$.

Comparing the $Q_{tot}/Q_{tot,IrO_2}$ ratios, it is evident that only in the case of materials prepared by co-synthesis (Alk-Ir$_{CS}$) their values (0.19 and 0.13) closely resemble the molar fraction of IrO_2. In all other cases the ratio is always higher than the nominal composition, thus pointing to a higher availability of surface iridium sites.

This supports the adopted strategy for designing materials with high activity/cost ratios. In this sense, the most important parameter is the fraction of Ir sites that participate in reaction (1), *i.e.* the number of Ir sites that freely exchange protons with the solution.

These values are summarized in Fig. 3, together with the total number of site densities.

Interestingly, as already suggested in the literature[41] the amount of Ir sites involved in the electrochemical processes is, in the case of pure IrO_2, in the order of a few percentages. Similar values are shown by materials in which iridium is not concentrated at the surface (*e.g.* by CS), but is homogeneously dispersed into the tin oxide matrix, up to the extreme case in which a solid solution is formed.[30]

The best case is offered by materials in which IrO_2 is purportedly added after the tin xerogel synthesis: much higher percentages (more than 10%) of "useful" Ir sites are shown in the case of materials obtained by both impregnation and mechanical mixing. As highlighted by XPS and XRD results, these materials show the highest surface concentration of iridium (see Table 1, Ir/Sn from XPS).

Interestingly, we recently[42] disclosed the fine structure of these samples by demonstrating that the remaining portion of Ir is actually dissolved into the SnO_2 matrix. This results in a "symbiosis" between IrO_2 and SnO_2, that leads to materials that possess a surface concentration of Ir close to the one of pure IrO_2 powders and high electronic conductivity (iridium acts as a dopant of SnO_2), but contain a small percentage of the precious component.

Recalling that these results were achieved thanks to the use of C-MEs and to the exact knowledge of the amount of powder under investigation, it is interesting to discuss the trend exhibited by the Q_{tot} density (Fig. 3 blue circles), which parallels the fraction of useful sites for all samples, since they have the same nominal composition, but for the pure IrO_2, for which the large waste of precious material is evident.

Even more interesting conclusions can be drawn after further normalizing the specific amount of sites, $n_{s,tot}$ and $n_{s,out}$ (mol g^{-1}) with respect to the specific surface area (S_{BET}, m^2 g^{-1}), to obtain the moles of active Ir sites per unit of surface area ($\Gamma(IrO_2)$).

In other words, the results reported in Fig. 4 represent the intensive availability of sites that can exchange protons with the solution. This easily leads to the following conclusions:

-materials prepared by tin alkoxide and impregnation (Alk-Ir$_{IMP}$_450, Alk-Ir$_{IMP}$_500) are the most promising in terms

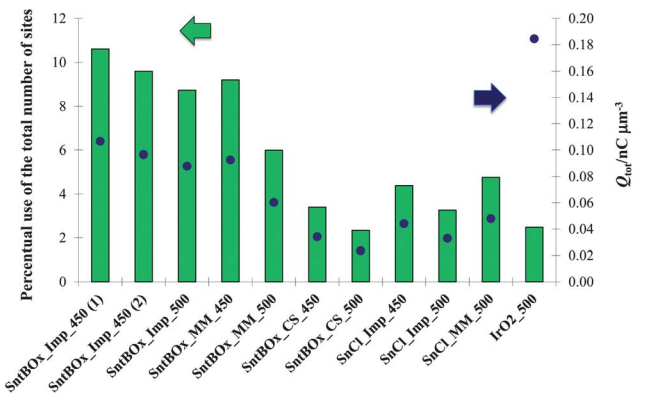

Fig. 3 Percentage of iridium sites effectively participating to pseudocapacitive phenomena, as obtained by integration of the voltammetric area (Q_{tot}), left axis, quantity of charge relevant to the density of "total" sites, right axis.

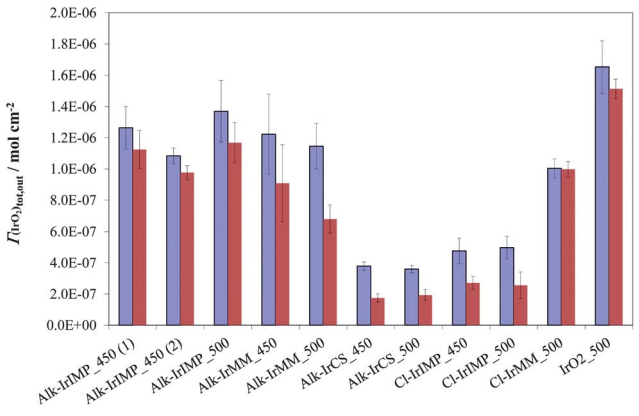

Fig. 4 Surface concentration of iridium sites participating to the pseudocapacitive phenomena. Error bars are meant to graphically represent the standard deviation values that are obtained adopting the error propagation theory.

of surface concentration of sites and exhibit a close behavior to pure IrO_2;

-the corresponding materials prepared by mechanical mixing represent the second choice in the rank, the lower number of most accessible sites points to the non-optimal dispersion of iridium oxide;

-in all cases the effect of the calcination temperatures is fully compensated by the normalization with the specific surface area values, leading to a preferential choice of the samples calcined at the lower T;

-the features of samples prepared by MM are independent of the nature of the tin precursor. In the case, instead, of the impregnation procedure, results show that samples obtained from the chloride precursor (Cl-Ir_{IMP}) present a lower availability of Ir (see XPS results, last column in Table 1), with respect to the corresponding sample from the alkoxide precursor (Alk-Ir_{IMP}).

We believe that during the impregnation step, in acidic environment, the tin xerogel from $SnCl_4$ could undergo partial dissolution/reorganization thus providing a loose matrix in which the iridium chloride might be absorbed and eventually included. This effect would therefore lower the amount of IrO_2 segregated at the surface of the particles that therefore behave more similarly to those prepared by co-synthesis.

Performance of membrane electrode assembly

The best material, Alk-Ir_{IMP}_450, chosen on the basis of its availability of active sites, its Q_{out}/Q_{tot} ratio, and the coverage of active sites, Γ, was used for the preparation of a membrane electrode assembly (MEA) that was tested at constant current density steps (1–10 kA m^{-2}), *i.e.* under real operative conditions. Moreover, and quite recently,[42] we have evaluated, by CV and by X-ray absorption measurements, the fine structure of most of the materials treated in the present work.

Interestingly, Alk-Ir_{IMP} materials are confirmed as the most promising ones. In fact, in these composites, Ir sites are mostly on the particles surface but also partially dissolved in the tin oxide matrix. This represents an optimal situation in terms of the number of Ir sites that are effectively active toward reactions (1) and (2): the active component on the surface is abundant and highly defective (different oxidation states were observed for surface Ir), while the portion dissolved in the matrix corresponds to the tin oxide doping that in turn leads to a high bulk electrical conductivity. We believe that this scenario (high availability of Ir, high defectivity of surface sites and high bulk conductance) is at the basis of the good performance shown in this work by Alk-Ir_{IMP_450}.

Fig. 5 shows the polarization characteristics recorded at different temperatures. The strong temperature effect points to the combined role of the increase of the ionic conductivity and of the electrode kinetics. At 80 °C, the whole cell requires a cell voltage of 1.9 V at 10 kA m^{-2}. This outcome is in line with the most promising results obtained in the last few years for low temperature solid polymer electrolyte water electrolyzers (SPEWE),[29,43,44] especially if considering the low loading of iridium oxide on the anode side of the MEA. It has to be noticed that the overall cell voltage includes the contributions of the cathode reaction and of uncompensated IR drops; nonetheless, the use of a well-known cathode material and solid polymer electrolyte allows direct correlation of this excellent performance to the anode electrocatalyst.

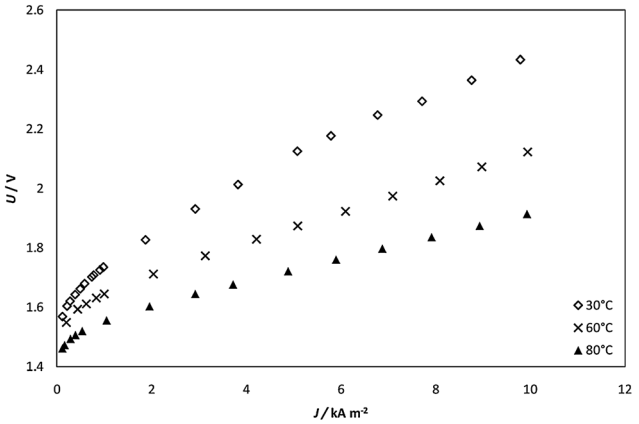

Fig. 5 Potential/current density (relevant to the geometric area) curves recorded under steady state conditions on the membrane/electrode assembly prepared using Alk-Ir_{IMP}_450 (1) as the anodic material.

Conclusions

In this paper, the use of cavity-microelectrodes for the quantitative rapid screening of catalytic materials has been analyzed and discussed in the case of mixed oxides to be used as anode catalysts for water electrolysis under acidic conditions. The screen procedure was applied to a matrix of IrO_2–SnO_2 powders with the same, low iridium percentage, whose synthetic methods differ in one or more parameters. In particular, some of the synthetic paths (mechanical mixing and impregnation) were aimed to enrich the final material surface with the highly active component while keeping the cost low.

The quantitative rapid screening allowed the characteristics of every material to emerge and rank them in terms of the number of sites able to exchange protons with the solution, sites that were proportional to those involved in the oxygen evolution reaction.[19]

This strategy is feasible, in the present work, since the difference in the intrinsic activity of different samples based on the same active component is rather similar (*e.g.* showing the same Tafel slope), as already proved by other authors in the particular case of iridium oxide-based catalysts.[45,46]

The method is obviously extendable to the screening and cross-comparison of materials having different active components (*e.g.* RuO_2, Co_3O_4, NiO, Pt, *etc.*). In this case, the mere characterization of the material in terms of the number of active sites should be accompanied by tests at water oxidation potentials performed still using C-MEs, as described in a previous publication.[19]

This makes the C-MEs so interesting in looking for a new promising material, especially from a set of samples that are quite similar in terms of nominal chemical composition but that differ in many other aspects. The choice of the best material therefore was not obvious: the list of different important properties (phase composition, surface and bulk composition, active component speciation, electrical conductivity and so on) is so long that is hard to predict the final behavior of the material without a strict,

quantitative method that allows quantification of the real number of available sites per unit surface area. That is why the C-ME represented an excellent tool for the purpose of this work.

The best material, Alk-Ir_{IMP}_450, was then used to prepare an operative membrane/electrode assembly that was tested in a solid polymer electrolyzer. The results highlighted the impressive performance of this material: the cell required 1.9 V for the passage of 10 kA m^{-2}.

Acknowledgements

We are grateful to Prof. A. J. Bard (The University of Texas at Austin) for fruitful discussions. Financial support from the Ministry of Education, University and Research (PRIN 2008PF9TWZ and 2008N7CYL5), Cariplo Foundation (project CARIPLO2010-0506) and Università degli Studi di Milano (PUR 2009) are gratefully acknowledged. A.M. and C.L. are thankful to the Università degli Studi di Milano for post-doc fellowships. C.L. is grateful to Fondazione Oronzio e Niccolò DeNora for a Scholarship in Electrochemistry.

References

1 A. J. Bard, *J. Am. Chem. Soc.*, 2010, **132**, 7559.
2 A. Wang, Y.-F. Huang, U. K. Sur, D.-Y. Wu, B. Ren, S. Rondinini, Ch. Amatore and Z.-Q. Tian, *J. Am. Chem. Soc.*, 2010, **132**, 17199.
3 Y.-F. Huang, D.-Y. Wu, A. Wang, B. Ren, S. Rondinini, Z.-Q. Tian and Ch. Amatore, *J. Am. Chem. Soc.*, 2010, **132**, 9534.
4 A. Minguzzi, M. A. Alpuche-Aviles, J. Rodriguez Lopez, S. Rondinini and A. J. Bard, *Anal. Chem.*, 2008, **80**, 4055.
5 J. L. Fernández, D. A. Walsh and A. J. Bard, *J. Am. Chem. Soc.*, 2005, **127**, 357.
6 J. Lee, H. Ye, S. Pan and A. J. Bard, *Anal. Chem.*, 2008, **80**, 7445.
7 M. Woodhouse and B. A. Parkinson, *Chem. Mater.*, 2008, **20**, 2495.
8 C.-L. Lin, C. M. Sanchez-Sanchez and A. J. Bard, *Electrochem. Solid-State Lett.*, 2008, **11**, B136.
9 C. Jung, C. M. Sanchez-Sanchez, C.-L. Lin, J. Rodriguez-Lopez and A. J. Bard, *Anal. Chem.*, 2009, **81**, 7003.
10 J. Rodriguez-Lopez, M. A. Alpuche-Avilés and A. J. Bard, *Anal. Chem.*, 2008, **80**, 1813.
11 J. M. Gregoire, M. E. Tague, S. Cahen, S. Khan, H. D. Abruna, F. J. DiSalvo and R. B. van Dover, *Chem. Mater.*, 2010, **22**, 1080.
12 J. Rodriguez-Lopez, M. A. Alpuche-Avilés and A. J. Bard, *J. Am. Chem. Soc.*, 2008, **130**, 16985.
13 Q. Wang, J. Rodríguez-López and A. J. Bard, *J. Am. Chem. Soc.*, 2009, **131**, 17046.
14 J. Rodríguez-López and A. J. Bard, *J. Am. Chem. Soc.*, 2010, **132**, 5121.
15 J. Rodríguez-López, A. Minguzzi and A. J. Bard, *J. Phys. Chem. C*, 2010, **114**, 18645.
16 C. S. Cha, C. M. Li, H. X. Yang and P. F. Liu, *J. Electroanal. Chem.*, 1994, **368**, 47.
17 V. Vivier, S. Belair, C. Cachet-Vivier, C. S. Cha, J.-Y. Nedelec and L. T. Yu, *Electrochem. Commun.*, 2000, **2**, 180.
18 A. Vertova, R. Barhdadi, C. Cachet-Vivier, C. Locatelli, A. Minguzzi, J.-Y. Nedelec and S. Rondinini, *J. Appl. Electrochem.*, 2008, **38**, 965.
19 C. Locatelli, A. Minguzzi, A. Vertova, P. Cava and S. Rondinini, *Anal. Chem.*, 2011, **83**, 2819.
20 F. M. Sapountzi, S. C. Divane, E. I. Papaioannou, S. Souentie and C. G. Vayenas, *J. Electroanal. Chem.*, 2011, **662**, 116.
21 A. Marshall, B. Børresen, G. Hagen, M. Tsypkin and R. Tunold, *Electrochim. Acta*, 2006, **51**, 3161.
22 C. Costentin, M. Robert and J.-M. Saveant, *Chem. Rev.*, 2010, **110**, PR1.
23 S. J. Kwon, F.-R. F. Fan and A. J. Bard, *J. Am. Chem. Soc.*, 2010, **132**, 13165.
24 M. W. Kanan and D. G. Nocera, *Science*, 2008, **321**, 5892.
25 Y. Surendranath, M. Dinca and D. G. Nocera, *J. Am. Chem. Soc.*, 2009, **131**, 2615.
26 J. G. McAlpin, Y. Surendranath, M. Dincă, T. A. Stich, S. A. Stoian, W. H. Casey, D. G. Nocera and R. D. Britt, *J. Am. Chem. Soc.*, 2010, **132**, 6882.
27 T. Nakagawa, N. S. Bjorge and R. W. Murray, *J. Am. Chem. Soc.*, 2009, **131**, 15578.
28 A. Vertova, L. Borgese, G. Cappelletti, C. Locatelli, A. Minguzzi, C. Pezzoni and S. Rondinini, *J. Appl. Electrochem.*, 2008, **38**, 973.
29 L. Ma, S. Sui and Y. Zhai, *Int. J. Hydrogen Energy*, 2009, **34**, 678.
30 S. Ardizzone, C. L. Bianchi, L. Borgese, G. Cappelletti, C. Locatelli, A. Minguzzi, S. Rondinini, A. Vertova, P. C. Ricci, C. Cannas and A. Musinu, *J. Appl. Electrochem.*, 2009, **39**, 2093.
31 A. C. Larson and R. B. Von Dreele, *GSAS: General Structural Analysis System*, Los Alamos National Laboratory, Los Alamos, NM, 1994.
32 B. H. Toby, *J. Appl. Crystallogr.*, 2001, **34**, 210.
33 B. R. Ezzell, H. S. Burney, M. W. Sorenson, *US Pat.*, 4376030, 1983.
34 J. Rouquerol, F. Rouquerol and K. S. W. Sing, in *Adsorption by Powders and Porous Solids*, Academic Press, London, 1999.
35 E. P. Barrett, L. G. Joyner and P. H. Halenda, *J. Am. Chem. Soc.*, 1951, **73**, 373.
36 S. Ardizzone, G. Cappelletti, A. Minguzzi, S. Rondinini and A. Vertova, *J. Electroanal. Chem.*, 2008, **621**, 185.
37 C. P. De Pauli and S. Trasatti, *J. Electroanal. Chem.*, 2002, **538**, 145.
38 S. Ardizzone, G. Fregonara and S. Trasatti, *Electrochim. Acta*, 1990, **35**, 263.
39 G. Spinolo, S. Ardizzone and S. Trasatti, *J. Electroanal. Chem.*, 1997, **423**, 49.
40 A. Minguzzi, F.-R. F. Fan, A. Vertova, S. Rondinini and A. J. Bard, *Chem. Sci.*, 2012, **3**, 217–229.
41 S. Fierro, T. Nagel, H. Baltruschat and C. Comninellis, *Electrochem. Commun.*, 2007, **9**, 1969.
42 A. Minguzzi, C. Locatelli, G. Cappelletti, M. Scavini, A. Vertova, P. Ghigna and S. Rondinini, *J. Phys. Chem. A*, 2012, DOI: 10.1021/jp212310v.
43 Y. Zhang, C. Wang, N. Wan, Z. Liu and Z. Mao, *Electrochem. Commun.*, 2007, **9**, 667.
44 S. Siracusano, V. Baglio, A. Di Blasi, N. Briguglio, A. Stassi, R. Ornelas, E. Trifoni, V. Antonucci and A. S. Aricò, *Int. J. Hydrogen Energy*, 2010, **35**, 5558.
45 S. Fierro, A. Kapałka and Ch. Comninellis, *Electrochem. Commun.*, 2010, **12**, 172.
46 I. A. Lervik, M. Tsypkin, L.-E. Owe and S. Sunde, *J. Electroanal. Chem.*, 2010, **645**, 135.

